Tailoring Interfacial Effect in Multilayers With Dzyaloshinskii-Moriya Interaction by Helium Ion Irradiation

A. Sud
University College London
S. Tacchi
Istituto Officina dei Materiali del CNR (CNR-IOM), Sede Secondaria di Perugia, c/o Dipartimento di Fisica e Geologia, Universita di Perugia
D. Sagkovits
University College London
C. Barton
National Physical Laboratory
M. Sall
Spin-Ion Technologies
L. H. Diez
Centre de Nanosciences et de Nanotechnologies
E. Stylianidis
University College London
N. Smith
National Physical Laboratory
L. Wright
National Physical Laboratory
S. Zhang
King Abdullah University of Science and Technology Physical Sciences and Engineering Division
X. Zhang
King Abdullah University of Science and Technology Physical Sciences and Engineering Division
D. Ravelosona
Spin-Ion Technologies
G. Carlotti
Universita di Perugia
H. Kurebayashi
University College London
O. Kazakova
National Physical Laboratory

M. Cubukcu (murat.cubukcu@npl.co.uk)
National Physical Laboratory

Research Article

Keywords: Tailoring interfacial effect, multilayers, Dzyaloshinskii-Moriya, interaction, helium ion, irradiation, magnetic properties

Posted Date: June 17th, 2021

DOI: https://doi.org/10.21203/rs.3.rs-618455/v1

Version of Record: A version of this preprint was published at Scientific Reports on December 1st, 2021. See the published version at https://doi.org/10.1038/s41598-021-02902-y.

Tailoring interfacial effect in multilayers with Dzyaloshinskii-Moriya interaction by helium ion irradiation

A. Sud[1], S. Tacchi[2], D. Sagkovits[1,3], C. Barton[3], M. Sall[4], L. H. Diez[5], E. Stylianidis[1], N. Smith[3], L. Wright[3], S. Zhang[6], X. Zhang[6], D. Ravelosona[4,5], G. Carlotti[7], H. Kurebayashi[1], O. Kazakova[3], and M. Cubukcu[1,3,*]

[1]London Centre for Nanotechnology, University College London, 17-19 Gordon Street, London, WC1H 0AH, United Kingdom
[2]Istituto Officina dei Materiali del CNR (CNR-IOM), Sede Secondaria di Perugia, c/o Dipartimento di Fisica e Geologia, Università di Perugia, I-06123 Perugia, Italy
[3]National Physical Laboratory, Teddington, United Kingdom
[4]Spin-Ion Technologies, Palaiseau, France
[5]Centre de Nanosciences et de Nanotechnologies, Orsay, Île-de-France, France
[6]King Abdullah University of Science and Technology Physical Sciences and Engineering Division, Thuwal, Makkah, Saudi Arabia
[7]Dipartimento di Fisica e Geologia, Università di Perugia, Via Pascoli, I-06123, Perugia, Italy
[*]murat.cubukcu@npl.co.uk

ABSTRACT

We show a method to control magnetic interfacial effects in multilayers with Dzyaloshinskii-Moriya interaction (DMI) using helium (He^+) ion irradiation. We compare results from SQUID magnetometry, ferromagnetic resonance as well as Brillouin light scattering results on multilayers with DMI as a function of irradiation fluence to study the effect of irradiation on the magnetic properties of the multilayers. Our results show clear evidence of the He^+ irradiation effects on the magnetic properties which is consistent with interface modification due to the effects of the He^+ irradiation. This external degree of freedom offers promising perspectives to further improve the control of magnetic skyrmions in multilayers, that could push them towards integration in future technologies.

Introduction

Logic devices based on nano-magnetism show the capability to couple ultrafast reversal of the magnetic state (or bit) with a non-volatile nature due to high thermal stability. A promising magnetic memory architecture is domain-wall based racetrack memory where the bit is encoded in the form of magnetic domain-walls and moved by spin currents, is still struggling in its technological implementation. One of the main reasons is related to the pinning effects introduced by defects, limiting the dynamics and thus the energy cost to store the information[1,2]. Spintronic storage or logic based on magnetic skyrmions are anticipated to be more efficient and to have a higher storage capacities[3–13]. In fact, the small size of skyrmions allow for a significant reduction of the spacing between the bits and improves the ratio between the information flowing and the current density employed for the motion. The skyrmion topology, characterized by an integer whirling number[5], makes them particularly robust to the external environment and notably defects. Specifically, a multi-bit storage device using skyrmions as information carriers (bits), where the state of the device is modulated by an electric current that shifts the skyrmions in and out of the device. Such a behaviour, in which the state of the system (“weight") can be dynamically adapted to the environment, is analogous to a biological synapse and their synaptic plasticity[14]. This also opens a way for utilising such devices in novel applications, such as skyrmion-based artificial synapses and neuron type devices in low-power neuromorphic computing, or brain-inspired architectures for deep machine learning applications[15–20].

Indeed, materials lacking an inversion symmetry centre and with high spin-orbit coupling, can in general possess an additional term in the exchange energy, which is anti-symmetric; the Dyaloshinskii-Moriya interaction (DMI)[21,22]. This type of interaction favours the perpendicular alignment of adjacent spins and can lead to the formation of topological structures, such as skyrmions, possessing a particular chirality. When interfacial DMI in thin films is utilized for the formation of skyrmions, it is possible to tailor nucleation processes and skyrmion properties using a variety of approaches[23]. In this way, relevant magnetic properties, such as perpendicular magnetic anisotropy (PMA) or the DMI strength can be strongly modified. However, a method to reliably control the stability of skyrmions and their motion is still missing. One possible tool is the irradiation of magnetic multilayers by light irradiation using helium (He^+) ions[24].

In particular, it is possible to fine tune the PMA and DMI in ultrathin films and multilayers, which are dominated by interfacial effects, by appropriately adjusting the irradiation fluence[25–29]. Light He^+ ions, with energy of approximately 10 keV, are able to penetrate the stack, disturbing the atomic arrangement in their path and causing atoms to be slightly displaced, as He^+ ions end up deep inside the substrate[30]. This series of short-range interactions leads to a mild alteration of the magnetic properties of the material, without suffering from damage that would be caused by more aggressive techniques such as surface sputtering[25] or cascade collisions. This method has already been shown to modify the magnetic properties of ultrathin trilayers through soft intermixing[26,31,32].

Here, we present a way of controlling magnetic interfacial effects in multilayers exhibiting DMI using He^+ irradiation. We compare SQUID magnetometry, ferromagnetic resonance (FMR) and Brillouin light scattering (BLS) results on a set of Ta(4.5nm)/[Pt(4.5nm)/Co(1.2nm)/Ta(2.5nm)]$_{20}$ multilayers as a function of He^+ irradiation fluence (IR). We study the effect of the irradiation on the magnetic properties of multilayers such as magnetic anisotropy, Gilbert damping and DMI strength. Our results show clear evidence of the effect of He^+ irradiation on the magnetic properties which is consistent with a controllable interface modification. The ability to precisely tailor the magnetic properties by externally adjusting the properties of thin-films offers a promising way to control magnetic skyrmions, making them a viable option for future technological applications.

Results

SQUID magnetometry measurements

In order to investigate the magnetic properties such as the saturation magnetization M_s, the effective uniaxial anisotropy $K_{\mathrm{eff(SQUID)}}$ of the multilayers, we performed SQUID magnetometry at room temperature, applying an external field along the in-plane (hard-axis) and out-of-plane directions (easy-axis) with respect to the sample surface.

In Figures 1(a) and 1(b), we show the magnetization M as a function of the magnetic field $\mu_0 H$ in both orientations for different IR, which indicates that the easy axis lies along the normal to the sample. The saturation magnetization maintains a constant value M_s= 700 kA/m within the experimental error as a function of IR. The value of the effective out-of-plane magnetic anisotropy $K_{\mathrm{eff(SQUID)}} = K_\mathrm{u}^{\mathrm{eff(SQUID)}} - 1/2\mu_0 M_\mathrm{s}^2$ was estimated from the intersection of the slope of the initial magnetization curve with the saturation field, in the in-plane hysteresis loops (Fig.1(c))[33]. It contains both shape anisotropy - 1/2 $\mu_0 M_\mathrm{s}^2$ and the effective uniaxial anisotropy constant $K_\mathrm{u}^{\mathrm{eff(SQUID)}}$ which includes both the first (K_u) and second order contributions. The magnetic anisotropy field $\mu_0 H_{\mathrm{K}^{\mathrm{eff(SQUID)}}}$ was determined by $2K_\mathrm{u}^{\mathrm{eff(SQUID)}}/M_\mathrm{s}$, using the measured value M_s=700 kA/m. Both results $\mu_0 H_{\mathrm{K}^{\mathrm{eff(SQUID)}}}$ and $K_\mathrm{u}^{\mathrm{eff(SQUID)}}$ are summarized in Fig.1(d), as a function of increasing IR. These data clearly demonstrate a reduction of the magnetic anisotropy with increasing IR, until a certain level ($8 \times 10^{14} cm^{-2}$), where this decrease saturates. We attribute this change to the interfacial modification caused by the IR. When the sample is irradiated with He^+, atomic displacements are induced which affect the related magnetic properties[34]. By increasing the IR, the PMA is reduced due to induced intermixing at the interface[35–37]. The Pt/Co interface roughness (or intermixing) increases linearly with IR, resulting in a continuous reduction of interfacial PMA[35].

We could also determine $\mu_0 H_{\mathrm{K}^{\mathrm{eff(SQUID)}}}$, by the area enclosed between the out-of-plane and in-plane loops in one quadrant of the $M-H$ loops (see SI, Fig.S3). We have fair agreement of $K_\mathrm{u}^{\mathrm{eff(SQUID)}}$ between the results of Fig.1(d) and Fig.S3 in terms of IR dependence and values. A slight quantitative difference potentially comes from the fact that the one extracted by the area difference between in-plane and out-of-plane field sweeps contains contributions from multi-domain nature of the samples, which influence $M-H$ loops in small magnetic fields.

Ferromagnetic resonance (FMR) measurements

In order to understand the changes to the magnetic properties due to IR, FMR was employed (Fig.2(a)) to determine the effective magnetisation $\mu_0 M_{\mathrm{eff}}$, the effective anisotropy field $\mu_0 H_{\mathrm{K}^{\mathrm{eff(FMR)}}}$ and the Gilbert damping factor α of the multilayers. Figure 2(b) shows the typical FMR absorption spectra for the multilayers. The absorption peaks are fitted with symmetric and anti-symmetric Lorentzian functions at each frequency respectively. The fitting formula used to extract the parameters is given in Eq.S1 (see SI). By analysing these absorption peaks, the resonance position and the linewidth can be determined from which it is possible to obtain the dynamic properties for a given magnetic sample. The frequency dependent FMR results, (8 - 20 GHz), are shown in Fig.3(a-d) where the external field applied along the film normal for each IR sample.

The solid lines in Fig.3(a-d), are defined by least square fitting of the resonance condition: $f = \gamma\mu_0(H_{\mathrm{res}} - M_{\mathrm{eff}})/2\pi$ where γ is the gyromagnetic ratio, $\mu_0 M_{\mathrm{eff}} = \mu_0 M_\mathrm{s} - \mu_0 H_{\mathrm{K}^{\mathrm{eff(FMR)}}}$ the effective magnetization, respectively, and $\mu_0 H_{\mathrm{K}^{\mathrm{eff(FMR)}}} =$

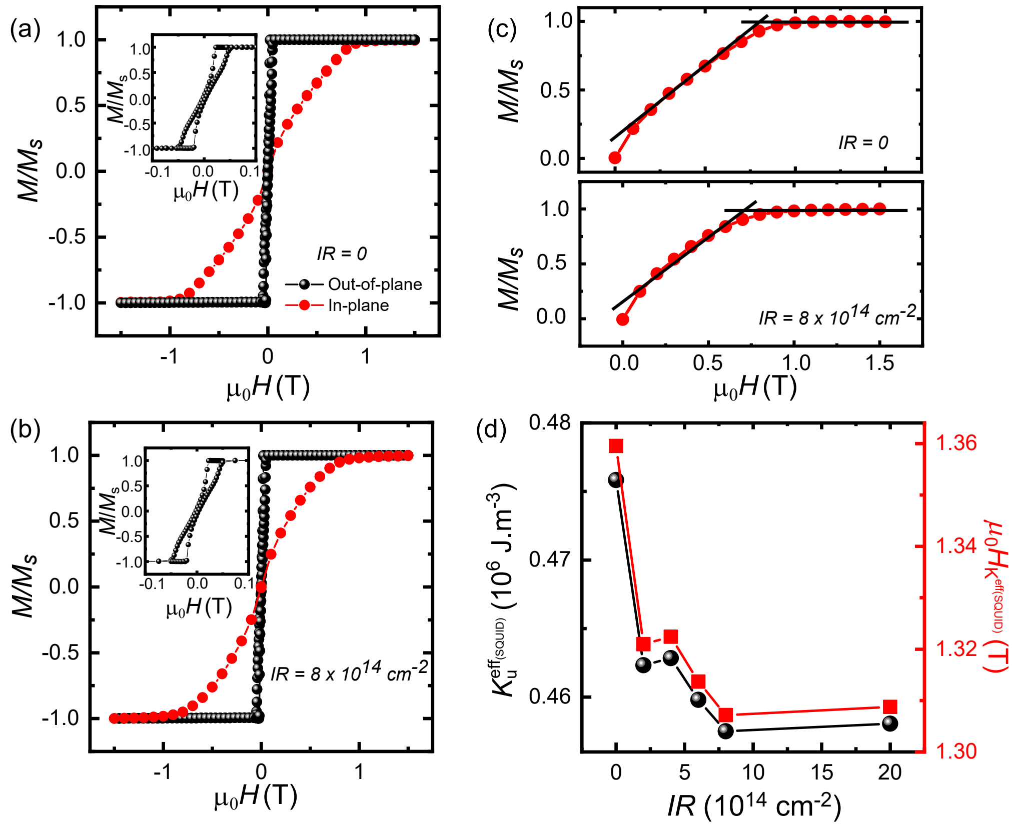

Figure 1. (a-b) Normalized magnetization measurements M/M_s while sweeping the external magnetic field $\mu_0 H$ in the direction perpendicular (out-of-plane) and parallel (in-plane) to the multilayers with different IR at room temperature. (c) Initial magnetization curve with in-plane orientation for different IR. In order to estimate the effective anisotropy field, we averaged the cross-section of a number of slopes taken along the curve from consecutive data points with the saturation field and we show here the average. (d) Effective anisotropy constant $K_u^{\text{eff(SQUID)}}$ and effective field $\mu_0 H_{K^{\text{eff(SQUID)}}}$ for different IR.

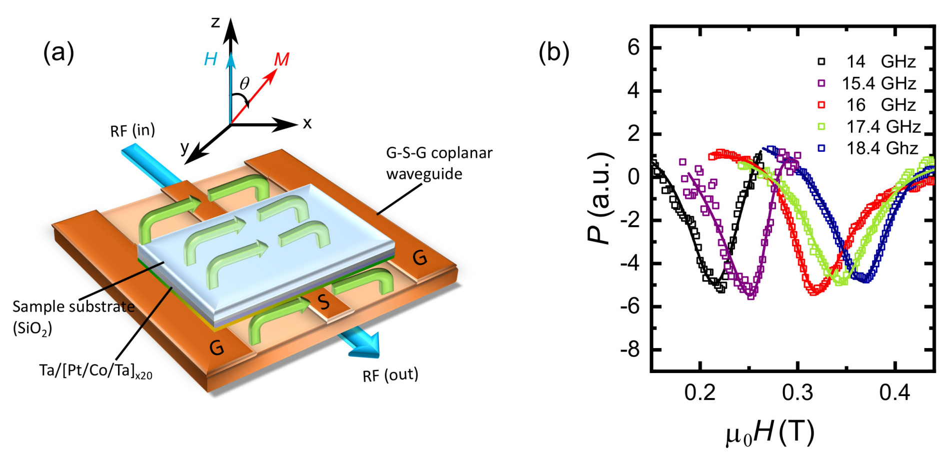

Figure 2. (a) Schematic illustration of FMR setup. (b) The FMR absorption spectras for the sample IR with $2 \times 10^{14} cm^{-2}$ at various frequencies.

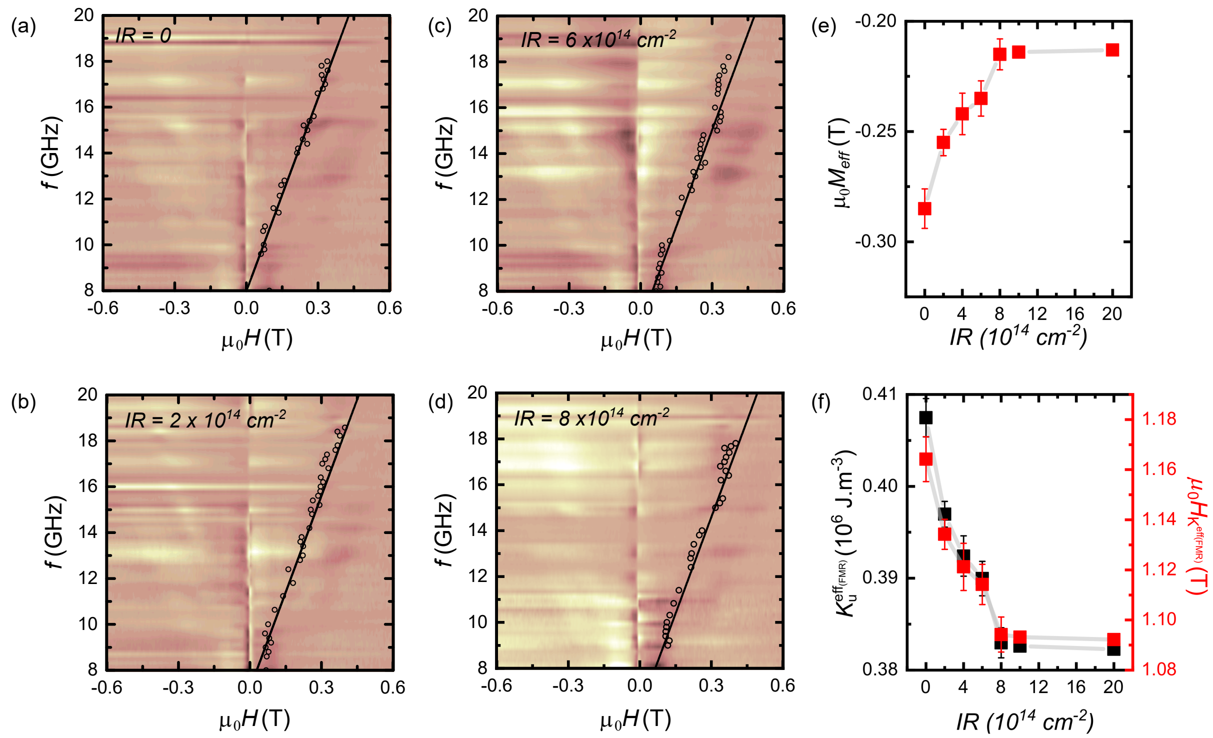

Figure 3. (a-d) Microwave transmission as a function of frequency for different IR with the magnetic field perpendicular to the film plane. The black hollow markers depict the resonance field obtained by fitting FMR spectra using the Eq. S1 and solid lines are fitting curve. (e-f) The effective magnetisation $\mu_0 M_{\text{eff}}$ (e) and the effective uniaxial anisotropy field $\mu_0 H_{\text{K}^{\text{eff}}(\text{FMR})}$ (f) as a function of IR.

$2K_{\text{u}}^{\text{eff}(\text{FMR})}/M_{\text{s}}$ is the effective uniaxial anisotropy field which includes first and second order magnetic anisotropy field contributions. We found that $\mu_0 M_{\text{eff}}$ is negative (Fig.3(e)), confirming that the demagnetizing energy is less than $\mu_0 H_{\text{K}^{\text{eff}}(\text{FMR})}$ giving rise to an easy-axis along the film normal (perpendicular easy-axis). The $\mu_0 M_{\text{eff}(\text{FMR})}$ value increases compared to non-irradiated sample as shown in Fig.3(e). Fig.3(f) details the evolution of both $\mu_0 H_{K^{\text{eff}}(\text{FMR})}$ and $K_{\text{u}}^{\text{eff}(\text{FMR})}$ as a function of increasing IR. As shown $\mu_0 H_{K^{\text{eff}}(\text{FMR})}$ and $K_{\text{u}}^{\text{eff}(\text{FMR})}$ rapidly decrease upon increasing the IR up to a saturation value occurring at a IR value of $\approx 8 \times 10^{14} cm^{-2}$. Thus, we show that an increase in IR can tailor the $\mu_0 H_{\text{K}^{\text{eff}}(\text{FMR})}$ of the multilayers. This behavior is in qualitative agreement with that obtained by analysing the hysteresis loops measured by SQUID. We also comment on the discrepancy in the anisotropy values obtained by SQUID magnetometry and FMR as evidenced. Due to the nature of the two measurement techniques it is somewhat expected that a small deviation in the values might be obtained. Such a discrepancy can be attributed to the fact that FMR results refer to the samples in the saturated and uniform ground state, while during the hysteresis cycles measured by SQUID the samples undergo a reversal involving also inhomogeneous magnetization configurations.

Analysis of the FMR linewidth $\mu_0 \Delta H$ is a generalized method for extracting α, which characterises the frequency dependent contribution to the Gilbert damping, as well as the inhomogeneous frequency independent contributions to the linewidth. Fig.4(a-d) shows the frequency dependence of linewidth $\mu_0 \Delta H$ for different IR. The extrinsic contributions to linewidth: magnetic inhomogeneity and two-magnon scattering can broaden the linewidth and cause a non-linear frequency dependence. The two-magnon contribution as a cause of linewidth broadening is ruled out since the measurements were performed along the out-of-plane direction where two-magnon processes are forbidden, according to Arias-Mills theory. The data is fitted using Gilbert damping contribution and frequency independent inhomogeneous contribution using the relation, $\mu_0 \Delta H = \mu_0 \Delta H_0 + 2\pi\alpha f/\gamma$ where α is the Gilbert damping contribution and $\mu_0 \Delta H_0$ is the extrinsic contribution present due to inhomogeneities. It can be seen from Fig.4(e) that the α value gradually increases as the IR is increased and saturates at a certain level. This shows that the presence of radiation affects the relaxation rate, but the inhomogeneous contribution is almost constant for all the samples within the error bars (Fig.4(f)).

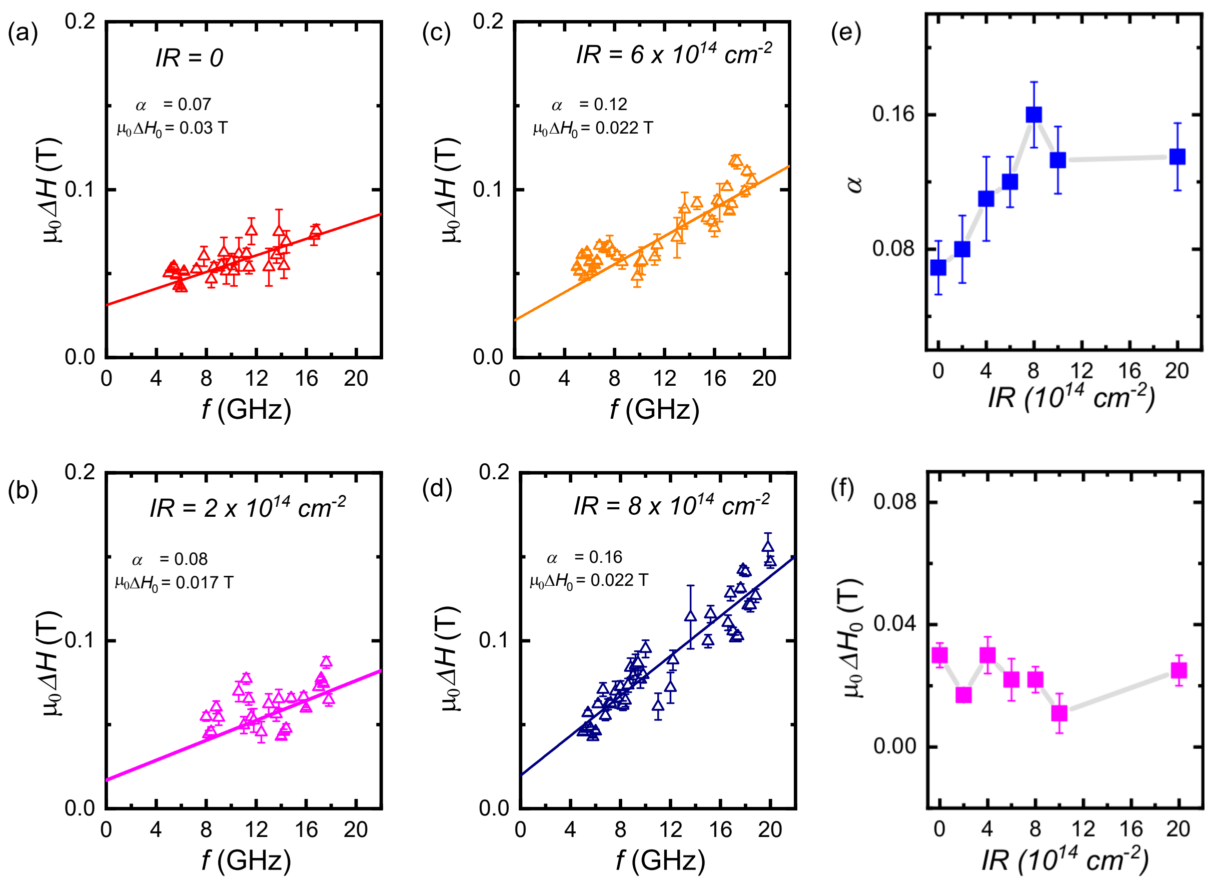

Figure 4. (a-d) Dependence of the linewidth, $\mu_0\Delta H$, on the microwave frequency, *f*, with in the out-of-plane external magnetic field $\mu_0 H$ for different IR. The solid lines are linear fits. (e) Plot of damping constant α and (f) Inhomogeneous broadening component $\mu_0\Delta H_0$ for different IR.

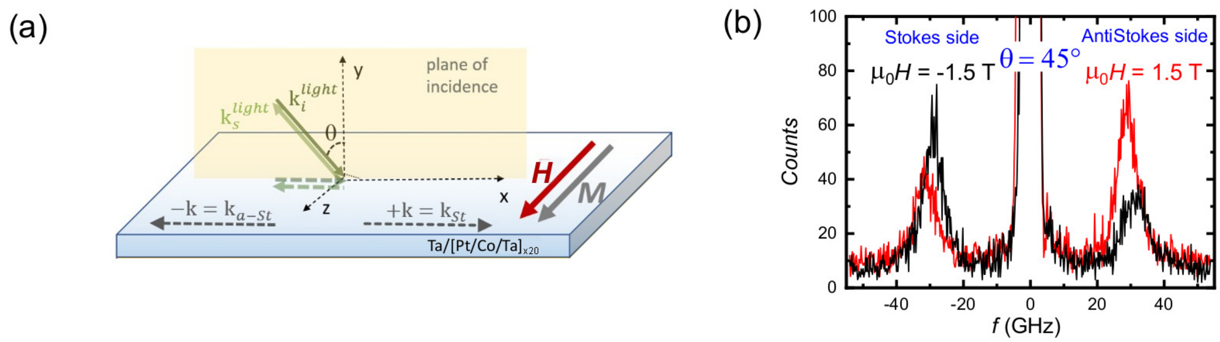

Figure 5. (a) Schematic of Brillouin light scattering (BLS) experiment. The sample is saturated in-plane by an external field $\mu_0 H$ = 1.5 T, applied along the z-axis. Stokes and anti-Stokes events in the scattering process correspond to spin waves propagating with +k and -k, respectively. (b) BLS spectra measured on the as-grown sample at an angle of incidence 45°, applying an in-plane field $\mu_0 H$ = ±1.5 T.

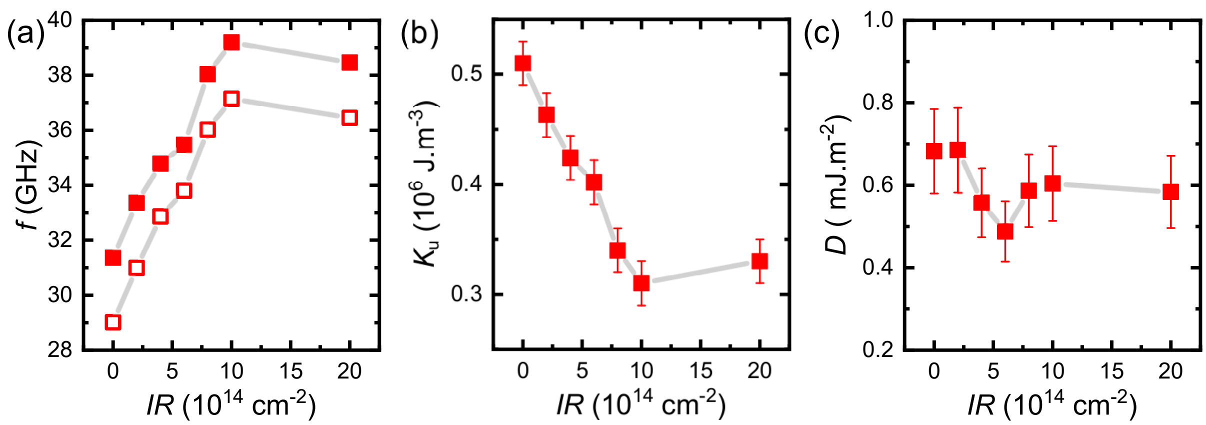

Figure 6. (a) Evolution of the absolute values of the Stokes (full dots) and anti-Stokes (open dots) frequencies measured for positive applied field $\mu_0 H$ = 1.5 T, as a function of the IR. (b) The first order out-of-plane uniaxial anisotropy constant (K_u) as a function of the IR. (c) Values of the DMI constant $D = (\pi M_s \Delta f)/2\gamma k$ derived from the frequency asymmetry between the anti-Stokes and Stokes peaks Δf of the Fig. 6(a).

Brillouin light scattering (BLS) measurements

As a final step in our investigation of the modifications of the magnetic properties of our multilayers induced by ion irradiation, we exploited Brillouin light scattering (BLS) with in-plane saturated samples. BLS analysis permitted us to achieve a complementary estimation of the out-of-plane anisotropy constant, and also to obtain a quantitative evaluation of the DMI strength. An in-plane magnetic field $\mu_0 H$ = 1.5 T, sufficiently large to saturate the magnetization in the film plane, was applied along the z axis, while the in-plane k was swept along the perpendicular direction (x-axis), corresponding to the Damon-Eshbach (DE) geometry (Fig.5(a)). Due to the conservation of momentum in the light scattering process, the magnitude of the spin wave wavevector k is related to the incidence angle of light θ, by the relation $k = 4\pi \sin\theta/\lambda$. Interfacial DMI induces a frequency asymmetry between DE modes propagating in opposite in-plane directions, corresponding to either Stokes or anti-Stokes peaks in BLS spectra (Fig.5(b)), perpendicular to the sample magnetization, following the relation $\Delta f = 2\gamma D/(\pi M_s)k$, where D is the effective DMI constant, k is the spin wave vector, and γ is the gyromagnetic ratio. In order to estimate the effective DMI constant D, the spin wave frequency Δf was measured at $k = 1.67\times10^7$ rad/m (corresponding to $\theta = 45°$) on reversing the direction of the applied magnetic field, that is equivalent to the reversal of the propagation direction of the DE spin wave mode. Fig.5(b) shows BLS spectra measured for the as-grown sample. One can observe that the Stokes and anti-Stokes peaks are characterized by a sizeable frequency asymmetry, which reverses upon reversing the direction of the applied magnetic field.

In Fig.6(a) we show the evolution of the absolute values of the Stokes and anti-Stokes frequencies measured for positive applied field $\mu_0 H$ = 1.5 T, as a function of the IR. It is evident that there is an increase of the frequencies with the IR, reflecting an increase of the effective magnetization of the stacks due to a reduction of the out-of-plane anisotropy. Fig.6(b) shows the values of the first order uniaxial anisotropy constant K_u obtained from the fit of the BLS frequency performed using the following expression that is valid for in-plane magnetized films of thickness t:

$$
\begin{aligned}
f(k) &= f_0(k) \pm f_{\mathrm{DMI}}(k) \\
&= \frac{\gamma\mu_0}{2\pi}\sqrt{H + Jk^2 + P(kt)M_s\left(H - \frac{2K_u}{M_s} + Jk^2 + M_s - P(kt)M_s\right)} \pm \frac{\gamma}{\pi M_s}Dk
\end{aligned}
\tag{1}
$$

Where J is the effective exchange constant and the dipolar term $P(kt)$, in the present case of an ultrathin film, becomes $\frac{|kt|}{2}$.

Discussion

He^+ irradiation shows a profound effect on the relaxation properties as demonstrated by a non-monotonic increase in damping value α (Fig.4e). The large damping parameter in these films can be attributed to an increase in surface magnon-electron interaction due to a large number of interfaces causing subsequent spin relaxation of conduction electrons that leave the Co layer at the various interfaces[38,39]. Furthermore, the effect of irradiation on damping in our multilayers indicates that the change in damping with IR can be correlated to a change in resistivity of the multilayers (see SI, S3). The dominant magnetization relaxation in our films involves electron scattering both in the bulk and also at the interfaces. To quantify the effect of scattering as the dominant mechanism, we measure the resistivity of the samples (Fig.S2). We find a correlation between resistivity and damping values, both showing an increase with increasing IR. The changes in ρ reflect the corresponding changes in α. The results signify a large contribution of electron scattering on the relaxation properties of He^+ irradiated multilayers.

In agreement with the SQUID and FMR results, K_u from BLS is observed to rapidly decrease on increasing IR (Fig.6(b)). One can note that for low IR values the K_u from BLS is larger than the effective uniaxial anisotropy constant obtained from FMR measurements (Fig.3(f)). This indicates that a negative contribution of the second order uniaxial anisotropy term (see SI, Fig. S4), favoring an in-plane easy-axis of the magnetization, is present. As can be seen in Fig.S4, the second order uniaxial anisotropy term is negative and its modulus decreases reaching an almost zero value at high IR. In Fig.6(c) we show the values of the DMI constant $D = (\pi M_s \Delta f)/2\gamma k$ derived from the frequency asymmetry Δf of the Fig.6(a). The positive value of D indicates that the right-handed chirality is favored by the DMI. As IR increases, a reduction of the DMI is observed at low IR followed by a non-monotonic increase with minima at IR = $6 \times 10^{14} cm^{-2}$. *Ab initio* calculations predict that intermixing at the Pt/Co interface results in a slight diminution of the DMI[40], in good agreement with our experimental results. A similar decrease with the He^+ irradiation was experimentally observed in W/CoFeB/MgO ultrathin films[32], although an increase was reported in Ta/CoFeB/Pt[29] and Ta/CoFeB/MgO[27,41].

In summary, we have demonstrated the control of the interfacial properties in Ta(4.5 nm)/$[$Pt(4.5nm)/Co(1.2nm)/Ta(2.5nm)$]_{20}$ multilayers with DMI caused to the sample by the He^+ irradiation using SQUID magnetometry, FMR and BLS. Our results show clear evidence of i) tailoring of interface ii) different magnetic properties in multilayers with different IR. As the IR increases, we observe that the PMA decreases significantly but after the IR reaches a certain level, it approaches saturation, while a reduction of the DMI is observed at low IR followed by a slight increase at larger IR. The He^+ irradiation induces short range atomic displacements, of the order of a few interatomic distances, leading to interface intermixing and hence altering the interface-driven PMA and DMI[31,42]. Moreover, He^+ irradiation also shows a profound effect on the relaxation properties as demonstrated by a non-monotonic increase in damping value α. We see a correlation between resistivity and damping values. The results signify a large contribution of electron scattering on the relaxation properties He^+ irradiated multilayers. Moreover, He^+ irradiation can be used virtually in any kind of ultra-thin materials, including ferrimagnets[43–45] and synthetic antiferromagnets[46]. In this way, we experimentally demonstrate a method to externally tune the control of skyrmionic ultra-thin films, bringing them one step closer to technological readiness in applications.

Methods

Sample preparation

The multilayers Ta(4.5 nm)/$[$Pt(4.5nm)/Co(1.2nm)/Ta(2.5nm)$]_{20}$ (see SI, Fig. S1 and table I) were deposited simultaneously on oxidized Si substrates by DC magnetron sputtering at room temperature. They were then uniformly irradiated at room temperature using a He^+-S system from Spin-Ion Technologies with a 25 keV He^+ beam at different IR.

Ferromagnetic resonance (FMR)

The measurements were performed by placing the magnetic multilayers on a co-planar wave-guide that generates the microwave magnetic fields at various frequencies and allows for the measurement of the absorbed power in the multilayers whilst sweeping the external field. The external field was modulated with an amplitude of a few mT at 12 Hz and phase-sensitive detection was used to increase the signal to noise ratio.

Brillouin light scattering (BLS)

BLS measurements were performed by focusing 150 mW of monochromatic light onto the sample surface. This was achieved using a single-mode diode-pumped solid state laser operating at λ = 532 nm, using a camera objective of f-number 1.8 and focal length 50 mm. The backscattered light was analyzed by a Sandercock-type (3-3)-pass tandem Fabry–Perot interferometer.

References

1. Parkin, S. S., Hayashi, M. & Thomas, L. Magnetic domain-wall racetrack memory. Science **320**, 190–194 (2008).
2. Parkin, S. & Yang, S.-H. Memory on the racetrack. Nat. Nanotechnol. **10**, 195–198 (2015).
3. Roessler, U. K., Bogdanov, A. & Pfleiderer, C. Spontaneous skyrmion ground states in magnetic metals. Nature **442**, 797–801 (2006).
4. Mühlbauer, S. et al. Skyrmion lattice in a chiral magnet. Science **323**, 915–919 (2009).
5. Nagaosa, N. & Tokura, Y. Topological properties and dynamics of magnetic skyrmions. Nat. nanotechnology **8**, 899–911 (2013).
6. Fert, A., Cros, V. & Sampaio, J. Skyrmions on the track. Nat. nanotechnology **8**, 152–156 (2013).
7. Moreau-Luchaire, C. et al. Additive interfacial chiral interaction in multilayers for stabilization of small individual skyrmions at room temperature. Nat. nanotechnology **11**, 444–448 (2016).
8. Boulle, O. et al. Room-temperature chiral magnetic skyrmions in ultrathin magnetic nanostructures. Nat. nanotechnology **11**, 449 (2016).
9. Woo, S. et al. Observation of room-temperature magnetic skyrmions and their current-driven dynamics in ultrathin metallic ferromagnets. Nat. materials **15**, 501–506 (2016).
10. Das, S. et al. Observation of room-temperature polar skyrmions. Nature **568**, 368–372 (2019).
11. Srivastava, T. et al. Large-voltage tuning of dzyaloshinskii–moriya interactions: A route toward dynamic control of skyrmion chirality. Nano letters **18**, 4871–4877 (2018).
12. Schott, M. et al. The skyrmion switch: turning magnetic skyrmion bubbles on and off with an electric field. Nano letters **17**, 3006–3012 (2017).
13. Cubukcu, M. et al. Electrical nucleation and detection of single 360° homochiral néel domain walls measured using the anomalous nernst effect. Appl. Phys. Lett. **112**, 262409 (2018).
14. Huang, Y., Kang, W., Zhang, X., Zhou, Y. & Zhao, W. Magnetic skyrmion-based synaptic devices. Nanotechnology **28**, 08LT02 (2017).
15. Li, S. et al. Magnetic skyrmion-based artificial neuron device. Nanotechnology **28**, 31LT01 (2017).
16. Grollier, J., Querlioz, D. & Stiles, M. D. Spintronic nanodevices for bioinspired computing. Proc. IEEE **104**, 2024–2039 (2016).
17. Huang, Y. et al. Interface control of domain wall depinning field. AIP Adv. **8**, 056314 (2018).
18. Zhang, X., Zhou, Y. & Ezawa, M. Magnetic bilayer-skyrmions without skyrmion hall effect. Nat. communications **7**, 1–7 (2016).
19. Chen, X. et al. A compact skyrmionic leaky–integrate–fire spiking neuron device. Nanoscale **10**, 6139–6146 (2018).
20. Chen, M., Sengupta, A. & Roy, K. Magnetic skyrmion as a spintronic deep learning spiking neuron processor. IEEE Transactions on Magn. **54**, 1–7 (2018).
21. Moriya, T. Anisotropic superexchange interaction and weak ferromagnetism. Phys. review **120**, 91 (1960).
22. Dzyaloshinsky, I. A thermodynamic theory of "weak" ferromagnetism of antiferromagnetics. J. Phys. Chem. Solids **4**, 241–255 (1958).
23. Cubukcu, M. et al. Dzyaloshinskii-moriya anisotropy in nanomagnets with in-plane magnetization. Phys. Rev. B **93**, 020401 (2016).
24. Juge, R. et al. Helium ions put magnetic skyrmions on the track. Nano Lett. **21**, 2989–2996 (2021).
25. Balk, A. L. et al. Simultaneous control of the dzyaloshinskii-moriya interaction and magnetic anisotropy in nanomagnetic trilayers. Phys. review letters **119**, 077205 (2017).

26. Herrera Diez, L. et al. Controlling magnetic domain wall motion in the creep regime in He^+-irradiated CoFeB/MgO films with perpendicular anisotropy. Appl. Phys. Lett. **107**, 032401 (2015).

27. Diez, L. H. et al. Enhancement of the dzyaloshinskii-moriya interaction and domain wall velocity through interface intermixing in Ta/CoFeB/MgO. Phys. Rev. B **99**, 054431 (2019).

28. Devolder, T. et al. Irradiation-induced tailoring of the magnetism of CoFeB/MgO ultrathin films. J. applied Phys. **113**, 203912 (2013).

29. Nembach, H. T. et al. Tuning of the dzyaloshinskii-moriya interaction by He^+ ion irradiation. arXiv preprint arXiv:2008.06762 (2020).

30. Rettner, C., Anders, S., Baglin, J., Thomson, T. & Terris, B. Characterization of the magnetic modification of Co/Pt multilayer films by He^+, Ar^+, and Ga^+ ion irradiation. Appl. Phys. Lett. **80**, 279–281 (2002).

31. Chappert, C. et al. Planar patterned magnetic media obtained by ion irradiation. Science **280**, 1919–1922 (1998).

32. Zhao, X. et al. Enhancing domain wall velocity through interface intermixing in W-CoFeB-MgO films with perpendicular anisotropy. Appl. Phys. Lett. **115**, 122404 (2019).

33. Thomson, T., Lengsfield, B., Do, H. & Terris, B. Magnetic anisotropy and reversal mechanisms in dual layer exchanged coupled perpendicular media. J. Appl. Phys. **103**, 07F548 (2008).

34. King, J. et al. Local control of magnetic damping in ferromagnetic/non-magnetic bilayers by interfacial intermixing induced by focused ion-beam irradiation. Appl. physics letters **104**, 242410 (2014).

35. Devolder, T. Light ion irradiation of Co/Pt systems: Structural origin of the decrease in magnetic anisotropy. Phys. Rev. B **62**, 5794–5802 (2000).

36. Ravelosona, D. et al. Magnetic properties of irradiated highly anisotropic materials. IEEE Transactions on Magn. **37**, 1643–1645 (2001).

37. Hauet, T. et al. Influence of ion irradiation on switching field and switching field distribution in arrays of Co/Pd-based bit pattern media. Appl. Phys. Lett. **98**, 172506 (2011).

38. Ingvarsson, S. et al. Role of electron scattering in the magnetization relaxation of thin $Ni_{81}Fe_{19}$ films. Phys. Rev. B **66**, 214416 (2002).

39. Berger, L. Effect of interfaces on gilbert damping and ferromagnetic resonance linewidth in magnetic multilayers. J. Appl. Phys. **90**, 4632–4638 (2001).

40. Zimmermann, B. et al. Dzyaloshinskii-moriya interaction at disordered interfaces from ab initio theory: Robustness against intermixing and tunability through dusting. Appl. physics letters **113**, 232403 (2018).

41. Casiraghi, A. et al. Bloch-to-Néel domain wall transition evinced through morphology of magnetic bubble expansion in Ta/CoFeB/MgO layers. arXiv preprint arXiv:1907.03708 (2019).

42. Fassbender, J., Ravelosona, D. & Samson, Y. Tailoring magnetism by light-ion irradiation. J. Phys. D: Appl. Phys. **37**, R179 (2004).

43. Woo, S. et al. Current-driven dynamics and inhibition of the skyrmion hall effect of ferrimagnetic skyrmions in GdFeCo films. Nat. communications **9**, 1–8 (2018).

44. Caretta, L. et al. Fast current-driven domain walls and small skyrmions in a compensated ferrimagnet. Nat. nanotechnology **13**, 1154–1160 (2018).

45. Hirata, Y. et al. Vanishing skyrmion hall effect at the angular momentum compensation temperature of a ferrimagnet. Nat. nanotechnology **14**, 232–236 (2019).

46. Legrand, W. et al. Room-temperature stabilization of antiferromagnetic skyrmions in synthetic antiferromagnets. Nat. materials **19**, 34–42 (2020).

Acknowledgements

This project 17FUN08 TOPS has received funding from the EMPIR programme co-financed by the Participating States and from the European Union's Horizon 2020 research and innovation programme. This project was also supported by the UK government department for Business, Energy and Industrial Strategy through NMS funding (Low Loss Electronics) and the UK national Quantum Technologies programme. A. S. and D. S. thanks EPSRC for their supports through NPIF EPSRC Doctoral studentship (EP/R512400/1) and Centre for Doctoral Training in Advanced Characterisation of Materials (EP/L015277/1) respectively. We would like to thank Pavlo Zubko for fruitful discussions on the X-ray reflectivity measurements.

Author contributions statement

A.S. performed FMR measurements and A.S., M.C. analysed the results. S.T. and G.C. performed BLS measurements and analysed the results. M.C. performed SQUID magnetometry measurements and D.S., M.C. analysed the results. S. Z. and X. Z. fabricated, M.S., L.H.D. and D.R. irradiated samples. E.S. performed X-ray reflectivity measurements and analysed the results. C.B. performed MFM measurements and C.B. N.S., L.W. analysed the results. H.K. and O.K. contributed to the interpretation of the results. M.C., A.S. and S.T. wrote the manuscript with inputs from the other authors. M.C. supervised the project.

Additional information

Springer Nature remains neutral with regard to jurisdictional claims in published maps and institutional affiliations. **Supplementary Information**. **Competing interests** The authors declare no competing interests.

Supplementary Files

This is a list of supplementary files associated with this preprint. Click to download.

- IRSIMC.pdf